L. Porcelli, A. Pastor, A. Cano, G. Escribano, M. Sanjurjo-Rivo, D. Escobar, P. Di Lizia
Satellite Maneuver Detection and Estimation with Radar Survey Observations
Acta Astronautica, Published online 18/08/2022
doi:10.1016/j.actaastro.2022.08.021

Satellite maneuver detection and estimation with radar survey observations

Lorenzo Porcelli[a,*], Alejandro Pastor[a], Alejandro Cano[a], Guillermo Escribano[b], Manuel Sanjurjo-Rivo[b], Diego Escobar[a], Pierluigi Di Lizia[c]

[a] *GMV, Calle Isaac Newton 11, Tres Cantos, 28670, Madrid, Spain*
[b] *Universidad Carlos III de Madrid, Avenida de la Universidad 30, Leganés, 28911, Madrid, Spain*
[c] *Politecnico di Milano, Via Privata Giuseppe La Masa 34, Milan, 20156, Italy*

Abstract

The space environment is rapidly getting congested, inducing a growth of the risk of collision between Resident Space Objects (RSOs). The validity of collision risk assessment depends on the quality of the catalogs of RSOs, which shall be as accurate and up-to-date as possible. Maneuvers of operational satellites represent a problem, because, if not correctly detected and estimated, they could lead to catalog degradation or pollution. In this paper, a novel approach to tackle the maneuver detection and estimation problem is presented. The methodology, which is part of the association problem between tracks and objects, is intended to be included in real-time cataloging systems to increase their flexibility. This paper is a continuation, extension and improvement of a former work, where maneuver estimation was carried out with optical observations. The estimation algorithm is extended to radar observations with the inclusion of a new dynamical model. The joint detection and estimation scheme is tested in a simulated maintenance chain with tracks and orbits from a single satellite. In this scenario, the output of the maneuver estimation is then used as an a-priori guess in high-fidelity orbit determination, which is refined and used to compute a post-maneuver orbit. The results of the application of the detection and estimation algo-

*Corresponding author

Email addresses: lorenzo.porcelli@gmv.com (Lorenzo Porcelli), apastor@gmv.com (Alejandro Pastor), alcano@gmv.com (Alejandro Cano), guescrib@ing.uc3m.es (Guillermo Escribano), msanjurj@ing.uc3m.es (Manuel Sanjurjo-Rivo), descobar@gmv.com (Diego Escobar), pierluigi.dilizia@polimi.it (Pierluigi Di Lizia)

rithm within the simulated chain is presented, highlighting its advantages and validating the methodology, providing a basis for a wider multi-target multi-sensor association framework, with the final goal of solving the association problem with data from survey activities.

Keywords: maneuver detection, maneuver estimation, track association, uncorrelated tracks resolution, cataloging

---

1. Introduction

As space activities have thrived in recent years, the number of Resident Space Objects (RSOs) is facing a rapid and ever-increasing growth. The definition of RSO is attributed to both operational satellites and non-functional objects, commonly known as space debris. According to the latest Annual Space Environment Report issued by ESA in April 2022 [1], which summarizes and presents data collected for the Database and Information System Characterizing Objects in Space (DISCOS) [2], by the end of 2021 it was possible to count around 30,000 tracked RSOs orbiting the Earth. Of all of these objects, it is estimated that around 6,000 are active spacecrafts [3], with the majority of them having maneuvering capabilities. The most crowded region is the Low Earth Orbit (LEO), which spans in altitude from the Von Kármán line (approximately at 100 km) up to 2,000 km. This orbital belt is usually selected for satellite launches due to various scientific, technological and financial reasons. According to the latest Space Environment Annual report, around 60% of the total number of RSOs listed in DISCOS (approximately 18,000) were residing in LEO by the end of 2021. The major contribution to the growth of the number of objects in LEO can be attributed to the deployment of several constellations in this region [1]. In fact, it is already possible to count more than 2,300 Starlink, 420 OneWeb and the 75 Iridium-NEXT satellites [3]. The clustering of the LEO region has also been evidenced in the increasing number of conjunction alerts raised and collision avoidance maneuvers carried out [4]. Collisions between satellites or with other non-cooperative objects represent a great threat, as they might lead to fragmentation events in which spacecrafts get damaged or broken, eventually generating clouds of debris, in general hard to detect and track, and contributing to the congestion of space.

In order to keep the safest possible environment for space operations by improving collision risk assessment, there is a need to have frequently up-

dated and accurate orbital catalogs, that is, collections of well-established orbits describing the trajectories of RSOs. Cataloging activities, which are one of the major tasks in the discipline of Space Surveillance and Tracking (SST), consist in predicting and updating the orbits of objects already present in the catalogs, starting from observations, as well as detecting and estimating the motion of new objects. The main source of potential new object detection does not come from events that actually generate new RSOs (i.e. satellite launches or fragmentation), but rather from maneuvers [5]. The latter represent a puzzling problem in cataloging activities, because if not correctly detected and estimated, they can lead to a general loss of catalog accuracy and thus, reliability. In the case of survey activities, when new observations arrive to a cataloging system, they are generally correlated to existing orbits to determine the identity of the observed objects. In case a maneuver has occurred, any correlation will generally fail, especially for high magnitude burns and sufficiently after the maneuver epoch. Observations from post-maneuver states of an object could be eventually associated and, if a new object would be issued from the latter, that would represent a duplicate in the catalog. Regarding tracking activities, unaccounted maneuvers can generate observability issues in sensor tasking, because the target satellite would not be found in the predicted position and thus lead to a biased estimation of the orbital states.

The authors deem it necessary to clarify the nomenclature used in the following work and which may be different in the literature, especially for the tracking community. The term *track* is used to refer to a set of observations taken by a single sensor over a short period of time, originated from the same space object. An *observation* is instead a set of measurements taken at a specific time. Tracks from surveillance sensors are usually referred to as *uncorrelated tracks* (UCTs), since they do not provide information on the identity of the observed object. On the other hand, the term *orbit* refers to a well-established estimation of the state of an RSO, stored in a catalog.

The problem of maneuver detection and estimation for space objects has been tackled with different approaches. The early research in the field was focused on detecting anomalies within publicly available Two-Line Elements (TLEs). Some of the first works in this regard were presented by Patera [6] and by Kelecy et al. [7], in which the authors proposed the application of several time filters to TLE data sets to detect unexpected variations in the orbital elements triggered by maneuvers themselves. The most extensive literature on the topic however concerns applications with tracking data, with

many methodologies being classifiable as *maneuver detection filters* [8]. In general, these algorithms employ some performance metric for the detection of a maneuver, which is then included as a state variable to be estimated within sequential Orbit Determination (OD). For instance, Kelecy and Jah [9] proposed a method to detect in-track burns from high observation residuals and to later estimate their magnitude through an analytical formulation based on orbital elements; Vazquez et al. [8] suggested a detection metric computed via the state covariance (as a product of OD) and maneuver estimation with an Unscented Kalman Filter. Within this class of maneuver detection filters, the Multiple Models Adaptive Estimation (MMAE) is gaining popularity. The core of these techniques is to combine different dynamical models to describe the motion of a satellite accomplishing a maneuver. Examples can be found in Goff et al. [10], with a filter-through methodology based on Interactive Multiple Models (IMM), or in Ko and Scheeres [11], which made use of the Thrust Fourier Coefficients. Zucchelli et al. [12] developed an IMM estimation within a Multi Hypothesis Tracking (MHT) framework, in which uncertainty propagation is performed via a Multi Fidelity (MF) method. The latter combines a hierarchy of models with varying fidelity to obtain highly accurate yet fast predictions; in general, these methods make use of a few iterations of the most accurate (and therefore expensive) models, and many iterations of the least accurate, but fastest, models.

In applications with survey data, maneuver detection and estimation is usually incorporated in correlation problems involving observations and orbits. One of the key works was presented by Holzinger et al. [13], in which the maneuver detection and estimation problem is cast as an Optimal Control Problem (OCP), with the underlying assumptions that satellites generally perform maneuvers with the lowest propellant consumption. This methodology was soon resumed by Singh [14] and later by Serra et al. [15], who researched the topic within track-to-orbit association problems with optical observations. Here, the OCP is cast in the orbit space, as tracks are used for state estimation via Initial Orbit Determination (IOD) with the inclusion of admissible regions [16]. Other works developed in this field can fall into the category of *heuristics*, in which information about previous satellite maneuvers is characterized in a statistical manner and used to recognize repetitive patterns (typical in Geostationary Earth Orbit, or GEO) and solve the detection and estimation problem. In [17] and [18], the authors proposed a novel method which made use of a Kernel Density Estimator (KDE) to determine

the probability distribution function of post-maneuver states based on previous maneuver history; Escribano et al. [19, 20] also made use of such tool in a wider Stochastic Hybrid System framework, in which different information is fused to retrieve a maneuver estimate.

This paper presents a novel and operationally feasible algorithm targeting the LEO orbital regime, intended as an extension and adaptation of a previous publication by Pastor et. al [5]. In this former work, the maneuver detection and estimation problems are posed as part of an association problem between cataloged RSOs orbits, estimated some days before the maneuver, and a set of uncorrelated tracks, received afterwards. Due to the impact of a maneuver on orbital dynamics, most post-maneuver tracks will not be correlated against any object in the catalog. Such tracks, if compared to potential pre-maneuver orbits in the measurements space, will show high residuals, triggering the possible detection of a maneuver which is subsequently estimated via a batch-least squares method. Considering a multi-target association framework, a preliminary link, or *hypothesis*, represented by such maneuver can be established between the UCTs and an object (hence, a *track-to-orbit* association). Following this strategy, the detection time of a potential maneuver (i.e., the time to detect the maneuver since it was carried out) is considerably reduced since no new object initiation is performed.

The proposed maneuver detection and estimation algorithm does not require any a-priori information on the maneuver and is intended to be included as part of the cataloging chain of RSOs, in particular of the maintenance phase, to increase the capacity and flexibility of cataloging systems. In fact, the output of the estimation algorithm is an a-priori guess of the maneuver, which is used to update the cataloged orbit of the involved RSO. Nonetheless, the estimation of the post-maneuver orbit, as well as the one of the maneuver itself, has mediocre accuracy if only measurements from a single post-maneuver track are used, losing the ability to correlate future tracks against post-maneuver orbits via track-to-orbit correlation. Hence, the maneuver estimation process must be preceded by a track-to-track association step [21], used to cluster together enough post-maneuver tracks corresponding to the same RSO, allowing to reach estimation accuracy analogous to no-maneuver scenarios. Particular care is given to the run-time of the algorithm due to its foreseen application in an operational environment. In addition to the former work and to validate the proposed scheme, a simulation scenario resembling a cataloging maintenance chain including maneuver detection and

estimation is set up. Tests are performed considering tracks and the orbit of a single satellite, providing a clear understanding of the performances of the methodology, determining the impact of the number of tracks on the quality of estimation and serving as the basis for the development of the multi-target association framework.

Differently from the former work, focused on optical observations and thus mainly on the GEO regime, the subject of research of this paper is represented by radar observations, typical for observation in LEO. In fact, at the current technological level, optical telescopes are typically not suitable for sensing of LEO objects due to their fast motion [22]. On the other hand, radars cannot be employed for observing RSOs at high altitude as the required electromagnetic power, whose value increases with the fourth power of distance [23], would be excessive. As well as being faster, the dynamics of objects in LEO is subject to higher non-linearity and uncertainty than GEO: perturbations from Earth's gravitational field are stronger and aerodynamic drag, difficult to model and predict due to the changes in the atmospheric composition and in the spacecraft attitude [23], is non-negligible. Hence, a new dynamical model for the maneuver estimation process is presented, with the goal of improving the accuracy with respect to the former work, which relied on linear dynamics, while keeping the associated computational cost low, as required by the run-time requirements.

The paper is structured in 4 sections. Section 1 introduces the maneuver detection and estimation problem and its impact on SST activities, along with a short description of the state-of-the-art methodologies. Section 2 presents the developed methodology for maneuver detection and estimation, supported by its physical and mathematical framework, as well as the description of the proposed catalog maintenance scheme. Section 3 reports results obtained in the simulations, emphasizing the benefits and the limitations of the algorithms. Section 4 is dedicated to discussion and conclusions, to the description of the current status of the work, and finally to future developments.

2. Methodology

This section is divided into four subsections. The first one, Subsection 2.1, presents the logic behind the development of the maneuver detection scheme. Subsection 2.2 introduces the maneuver estimation algorithm. Subsection 2.3 shows the development of dynamical models to be used within the maneuver

estimation algorithm. Finally, Subsection 2.4 describes the proposed simulation scenario for catalog maintenance including maneuver detection and estimation starting from observations.

2.1. Maneuver detection

Let the pre-maneuver state under analysis, $\mathbf{y}_A(t)$, estimated with pre-maneuver tracks, be:

$$\mathbf{y}_A(t) = [\mathbf{x}_A(t), \mathbf{p}_A] \in \mathbb{R}^{(6+n_p)} \tag{1}$$

where $\mathbf{x}_A(t) \in \mathbb{R}^6$, is the aggregation of the position and velocity vectors, $\mathbf{r}_A(t) \in \mathbb{R}^3$ and $\mathbf{v}_A(t) \in \mathbb{R}^3$, respectively. On the other hand, the vector $\mathbf{p}_A \in \mathbb{R}^{n_p}$ is a set of dynamical parameters.

Consider now a potential post-maneuver track provided as input. This is a set of observations $\{\mathbf{z}_k\}$, where each observation $\mathbf{z}_k = \mathbf{z}(t_k)$ contains measurements taken at certain time t_k for $k = 1, \ldots, K$, with K being the total number of observations in the track. Each observation is made up of I types of measurements, defined by an index $i = 1, \ldots, I$. The selected metric for maneuver detection is the Weighted Root Mean Square (WRMS) of the track, referred to the i-th type of measurement, with respect to the pre-maneuver orbit:

$$WRMS_i = \sqrt{\frac{1}{K}\sum_{k=1}^{K}\left(\frac{\rho_{i,k}}{\sigma_i}\right)^2} \tag{2}$$

The term $\rho_{i,k} = z_{i,k} - h_i(t_k, \mathbf{x}_A(t_k))$ is the residual of the i-th measurement at the epoch of the k-th observation (t_k). The function $\mathbf{h}(t, \mathbf{x}_A(t))$ is the model that predicts measurements from the state vector of the pre-maneuver orbit. The term σ_i represents the standard deviation of the measurement i, quantifying the expected 1-sigma noise of the sensor for a given measurement type. A maneuver is expected to have occurred if one or more of the WRMS values of the track exceed a *threshold* defined as absolute threshold, meaning that an anomaly in the weighted residuals is being encountered. In fact, discrepancy between incoming observations and predicted ones is expected when satellites perform impulsive maneuvers, i.e., sudden changes in velocity. In case this is happening, the detection algorithm returns the input track by labeling it as a post-maneuver one. The scheme can

be applied equivalently to sets of multiple tracks, and in case providing the subset representing the post-maneuver tracks.

The selection of the value of the WRMS threshold is derived from a trade-off: it should be sufficiently low to always trigger true maneuver detection, but also sufficiently high to discard any possible outlier in the observations or noise in the dynamical model and avoid false maneuver detection. In fact, a challenging case for this approach is encountered when, in the case of low magnitude burns, the detection scheme is applied to a first post-maneuver track arriving closely to the maneuver epoch. As only a short time period after the maneuver has elapsed, the divergence of the residuals could be just interpreted as outliers and not be sufficiently high to exceed the threshold. For this reason, the detection methodology can be made more robust by applying a *secondary threshold* (as opposed to the *primary threshold*): if a post-maneuver track is detected through the primary threshold, the algorithm looks to the past to find previous tracks that exceed the secondary threshold. Since these past tracks are supposed to show a smaller divergence with respect to the one detected with the primary threshold, the value of the secondary threshold is expected to be lower than the primary. This strategy allows to retrieve all post-maneuver tracks and is beneficial for both the maneuver estimation process, since all of the relevant post-maneuver information can be used, but also for the re-estimation of the pre-maneuver orbit, as undetected post-maneuver track would contaminate the process.

The selection of the values for the thresholds, as well as the time interval to look for post-maneuver tracks into the past when applying the secondary thresholds, is discussed in Subsection 3.3. A scheme of the applied maneuver detection strategy is presented in Figure 1.

2.2. Maneuver estimation

The output of the maneuver detection scheme, when an anomaly in the observations is encountered, is a set of tracks labeled as post-maneuver. At a certain epoch, defined as t_M, an impulsive maneuver is assumed to take place. The pre-maneuver orbit $\mathbf{x}_A(t)$ will therefore drift towards a post-maneuver orbit $\mathbf{x}_B(t, \mathbf{u})$. Given the hypothesis of impulsive burn, the two orbits intersect at t_M, with their difference in velocity being the maneuver $\mathbf{u} \in \mathbb{R}^3$. The estimation algorithm was already introduced in [5] but it is summarized now for convenience. The goal is to find, for a fixed t_M, the maneuver which best fits the observations in a *least-squares* of the residuals sense (as represented

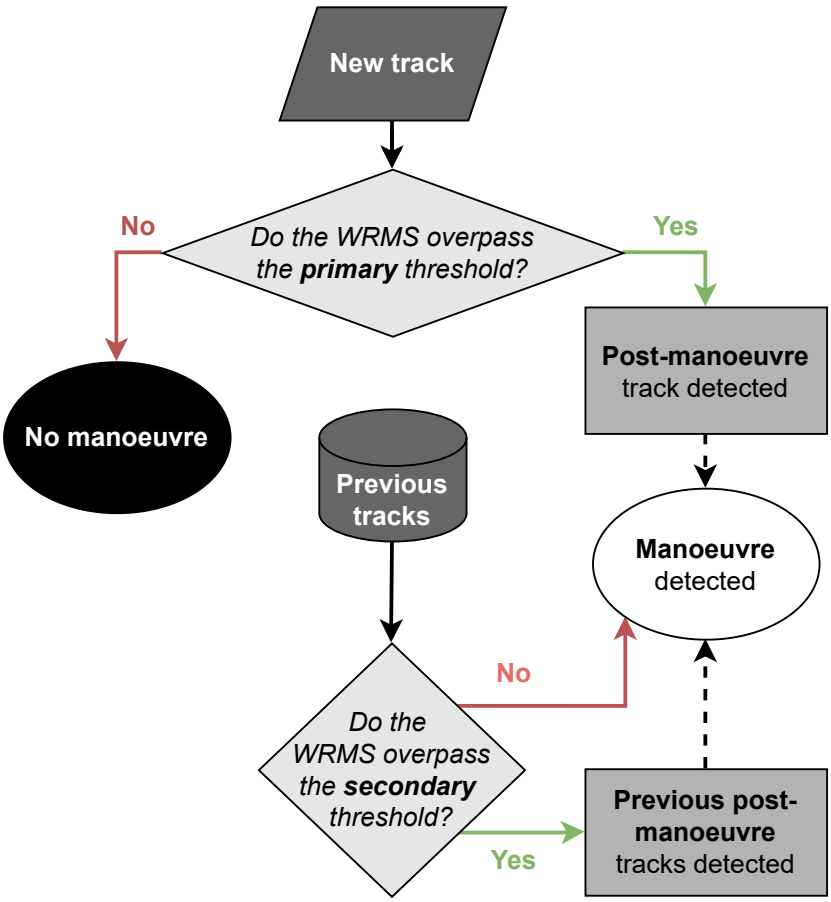

Figure 1: Maneuver detection scheme

in Figure 2). This is achieved by minimizing the following cost function, where $\boldsymbol{\rho}_l$ (for $l = 1, \ldots, L$) are the residuals:

$$J = \frac{1}{L} \sum_{l=1}^{L} \boldsymbol{\rho}_l^T \mathbf{W} \boldsymbol{\rho}_l \tag{3}$$

Or, equivalently, by the iterative solution of the following *normal equations* for $\Delta\mathbf{u} = \mathbf{u} - \mathbf{u}^*$:

$$\left(\mathbf{G}^T \mathbf{W} \mathbf{G}\right) \Delta\mathbf{u} = \left(\mathbf{G}^T \mathbf{W}\right) \Delta\mathbf{z} \tag{4}$$

$\sqrt{J}$ is the WRMS of all tracks involved in the estimation process. The matrix $\mathbf{W} \in \mathbb{R}^{I \times I}$ is the *weighting matrix*. $\Delta\mathbf{z} = \sum_l \mathbf{z}_l - \mathbf{h}\left(t_l, \mathbf{x}_B\left(t_l, \mathbf{u}^*\right)\right) \in$

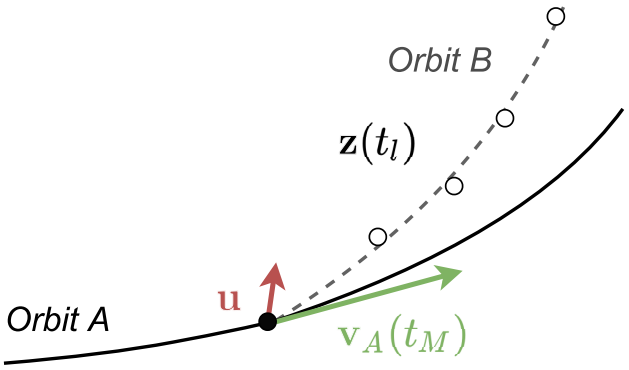

Figure 2: Representation of the maneuver estimation method

$\mathbb{R}^I$ (where t_l is the observation time) represents the difference between the actual measurements and those predicted from a reference trajectory $\mathbf{x}_B^*(t_l) = \mathbf{x}_B(t_l,\, \mathbf{u}^*)$. $\mathbf{G} \in \mathbb{R}^{I\times 3}$ is the *Jacobian*, which represents the partial derivatives of the measurements with respect to the estimated parameters. It can be computed as a sum of the contributions of each observation:

$$\begin{aligned}\mathbf{G} &= \sum_l \frac{\partial \mathbf{h}\left(t_l,\, \mathbf{x}_B\left(t_l,\, \mathbf{u}^*\right)\right)}{\partial \mathbf{u}} \\ &= \sum_l \frac{\partial \mathbf{h}\left(t_l,\, \mathbf{x}_B\left(t_l,\, \mathbf{u}^*\right)\right)}{\partial \mathbf{x}_B\left(t_l,\, \mathbf{u}\right))} \cdot \frac{\partial \mathbf{x}_B\left(t_l,\, \mathbf{u}^*\right)}{\partial \mathbf{u}}\end{aligned} \tag{5}$$

As the maneuver time is not known a-priori, the normal equations (Equation (4)) must be solved for a set of t_M values comprised in an interval T (from the last track used to estimate the pre-maneuver orbit to the first post-maneuver track being considered). Hence, the output of the algorithm is a pool of solutions for every $t_M \in T$, each one associated to a value of J (or, equivalently, $\sqrt{J}$) and to an estimated maneuver $\hat{\mathbf{u}}$. A simple strategy is proposed to retrieve the most suitable *a-priori estimate* (that is, a combination of $\hat{t}_M$ and $\hat{\mathbf{u}}$):

1. the global minimum in terms of the cost function (Equation (3)) is found and then just the solutions with a value of $\sqrt{J}$ *lower than the 110%* of the minimum are retained.
2. among this set, the solution associated to the *lowest control effort* $\|\hat{\mathbf{u}}\|$ (with $\|(\cdot)\|$ representing the norm of a vector) is selected.

$\sqrt{J}$ is selected as the leading metric for the short-listing as it quantifies the goodness of fit of the estimation problem. The rationale behind second step in the selection strategy is that, in the absence of further information, maneuvers performed by satellites are assumed to be optimal. The current percentage value for taking the solutions with minimum WRMS has proven to be a reasonable value, as it allows to locate the local minima regions and to account for the errors introduced by the discretization of T. The selection criterion is slightly different from the previous one [5], where the best solution was taken as the one with lowest $\|\hat{\mathbf{u}}\|$ but just among the local WRMS minima, without considering any margin for enlarging the pool. Nonetheless, the new proposed strategy can be applied also to GEO maneuver estimation, as it is able to retrieve the same estimates as the previous one. It is important to remark that this selection strategy is intended to be as simple as possible at deriving a reliable first estimate and is tailored to a single-satellite scenario. Further developments, aimed at extending the correlation problems to multiple RSOs, shall be posed in a multi-target association framework. In this regard, a possible approach would be to consider the solutions associated to the $\sqrt{J}$ minima as hypotheses and creating a set of hypotheses for each track-to-orbit association. These would be evaluated, pruned and eventually promoted through the analysis of subsequent post-maneuver tracks. In the catalog maintenance scheme, these a-priori estimates for maneuver time and size (in all three directions) are used in a high-fidelity orbit determination process, with a numerical propagator, which determines the post-maneuver orbit together with refining the initial maneuver guesses.

2.3. Development of dynamical models for maneuver estimation

Having set the physical and mathematical framework for maneuver estimation, the last step required is to define a dynamical model for $\mathbf{x}_B(t, \mathbf{u})$, required for the computation of the predicted measurements $\mathbf{h}(t, \mathbf{x}_B)$ and of the matrix $\mathbf{G}$ as a function of time and of maneuver size $\mathbf{u}$ (at a given maneuver time t_M). The requirement of computing multiple solutions for a set of t_M values before the final selection motivates the development and use of a computationally efficient propagation algorithm; the use of a typical numerical propagator would entail a very large computational cost, which is to be avoided considering the requirement of real time operation of the algorithm. For this reason, a simple, fast and yet sufficiently accurate dynamical model partially based on linear dynamics is developed. The model

is an improvement of the fully-linear one employed in maneuver estimation of GEO objects [5].

The *full state transition matrix* $\mathbf{\Psi}(t, t_0)$, relative to a reference time t_0, represents the linear mapping between the initial extended state vector $\mathbf{y}_A(t_0)$ and the extended state vector at any time t (both defined in Cartesian coordinates):

$$\mathbf{\Psi}(t,\, t_0) = \frac{\partial\, \mathbf{y}_A(t)}{\partial \mathbf{y}_A(t_0)} \in \mathbb{R}^{(6+n_p)\times(6+n_p)} \tag{6}$$

It can be conveniently subdivided into four sub-matrices [23]:

$$\mathbf{\Psi}(t, t_0) = \begin{bmatrix} \mathbf{\Phi}(t, t_0) & \mathbf{S}(t) \\ \mathbf{0} & \mathbb{I}_{n_p} \end{bmatrix} \tag{7}$$

With $\mathbf{\Phi}(t, t_0) \in \mathbb{R}^{6\times 6}$ and $\mathbf{S}(t) \in \mathbb{R}^{6\times n_p}$. The first sub-matrix is the so-called *state transition matrix* (STM), transition matrix of the position and velocity vectors with respect to the initial state, namely $\mathbf{\Phi}(t, t_0) = \partial \mathbf{x}_A(t)/\partial \mathbf{x}_A(t_0)$. The second term is the *sensitivity matrix*, the partial derivatives of the state vector with respect to the dynamical parameters: $\mathbf{S}(t) = \partial \mathbf{x}_A(t)/\partial \mathbf{p}_A$. On the other hand, $\mathbb{I}_{n_p}$ is the identity matrix of dimension $n_p \times n_p$.

The post-maneuver trajectory of $\mathbf{x}_B(t)$ can be found from a Taylor expansion with respect to a reference trajectory, such as $\mathbf{x}_A(t)$, and retaining at first only the zero and first order terms:

$$\mathbf{x}_B(t) \approx \mathbf{x}_A(t) + \frac{\partial \mathbf{x}_A}{\partial \mathbf{x}_A^0}(t) \cdot \left(\mathbf{x}_B^0 - \mathbf{x}_A^0\right) \tag{8}$$

$\mathbf{x}_A^0$ and $\mathbf{x}_B^0$ are the considered initial state of the two trajectories. Considering the beginning of the propagation at $t = t_M$, the difference between the initial states is simply equal to the maneuver $\mathbf{u}$, since:

$$\mathbf{x}_A^0 = \mathbf{x}_A(t = t_M) \tag{9a}$$

$$\mathbf{x}_B^0 = \mathbf{x}_B(t = t_M,\, \mathbf{u}) = \mathbf{x}_A^0 + [\mathbf{0},\, \mathbf{u}]^T \tag{9b}$$

The partial derivative $\partial \mathbf{x}_A(t)/\partial \mathbf{x}_A^0$ is the STM of trajectory A referred to t_M, namely $\mathbf{\Phi}(t,\, t_M)$, so the post-maneuver state at any time $t \geq t_M$ could be computed in linear dynamics (c.f. Pastor et al. [5]) as it follows:

$$\mathbf{x}_{B,lin}(t,\, t_M,\, \mathbf{u}) = \mathbf{x}_A(t) + \mathbf{\Phi}(t,\, t_M)_{\mathbf{xv}} \cdot \mathbf{u} \tag{10}$$

The subscript $(\cdot)_{\mathbf{xv}}$ represent the sub-matrix of the partial derivatives with respect to just the velocity components, as the difference in the two initial states does not have any position component.

The linear model can be extended by including the higher order effects of Keplerian dynamics. Hence, an improved dynamical model for the post-maneuver state can be written as:

$$\mathbf{x}'_B\left(t,\, t_M,\, \mathbf{u}\right) = \mathbf{x}_{B,lin}\left(t,\, t_M,\, \mathbf{u}\right) + \Delta\mathbf{x}_K\left(t,\, t_M,\, \mathbf{u}\right) \tag{11}$$

With:

$$\Delta\mathbf{x}_K\left(t,\, t_M,\, \mathbf{u}\right) = \mathbf{x}_{B,K}\left(t,\, t_M,\, \mathbf{u}\right) - \mathbf{x}_{A,K}\left(t,\, t_M\right) - \mathbf{\Phi}_{K,\mathbf{xv}}\left(t,\, t_M\right) \cdot \mathbf{u} \tag{12}$$

The states $\mathbf{x}_{A,K}\left(t,\, t_M\right)$ and $\mathbf{x}_{B,K}\left(t,\, t_M,\, \mathbf{u}\right)$ represent the two fully non-linear Keplerian trajectories, propagated from the initial states in Equations (9a) and (9b) respectively. The matrix $\mathbf{\Phi}_K\left(t,\, t_M\right)$ is instead the state transition matrix related to $\mathbf{x}_{A,K}\left(t,\, t_M\right)$, which can be computed analytically [23] or numerically via finite differences. This model will be named as *Keplerian + linear perturbations*. The equation can be further extended by expressing the higher order Keplerian effects in the local TNW (Transversal - Normal - Out-of-plane) frame:

$$\mathbf{x}_B\left(t,\, t_M,\, \mathbf{u}\right) = \mathbf{x}_{B,lin}\left(t,\, t_M,\, \mathbf{u}\right) + \mathbf{R}_{TNW}^T \cdot \mathbf{R}_{TNW,K} \cdot \Delta\mathbf{x}_K\left(t,\, t_M,\, \mathbf{u}\right) \tag{13}$$

The matrices $\mathbf{R}_{TNW}$ and $\mathbf{R}_{TNW,K}$ are the rotation matrices from the Cartesian frame to the local TNW frames associated with $\mathbf{x}_A\left(t\right)$ and $\mathbf{x}_{A,K}\left(t\right)$ respectively. For sake of simplicity, the expression for $\mathbf{x}_B\left(t,\, t_M,\, \mathbf{u}\right)$ will be defined as *Keplerian + linear perturbations with TNW corrections*, and will be the model employed in the maneuver estimation process. The normal equations matrix (Equation (5)) can be built up starting from the derivative of Equation (13) with respect to $\mathbf{u}$.

The reason behind the development of this enhanced version of the linear model is the foreseen application in LEO, where dynamics are faster and subject to higher non-linearity and uncertainty if compared to the GEO environment. In fact, with the simple linear model (Equation (10)), larger errors are expected for high-magnitude burns and for longer propagation times; this is particularly true for in-track burns, whose major effect is to change the

semi-major axis of the orbit (and therefore the orbital period). A test to determine the accuracy of the three presented dynamical models here proposed (linear, Keplerian + linear perturbations, Keplerian + linear perturbations with TNW corrections) will be presented in Subsection 3.1, highlighting the advantages of the last one with the other two. With respect to the linear model, the Keplerian + linear perturbations equations require the propagation of two Keplerian orbits and the computation of two state transition matrices at each integration step. However, via an efficient implementation of these two operations, the computational cost can be kept low, so not to impact the run-time performances of the maneuver estimation algorithm.

2.4. Catalog maintenance with maneuver detection and estimation

The proposed catalog maintenance scheme, depicted in Figure 3, accounts for maneuvers is tested and validated in a single-satellite tracking scenario. The goal is do determine the effectiveness and the performances of the detection and estimation algorithm, so to serve as basis for a development within multi-target multi-sensor association frameworks with data from surveillance activity. Each step of the process considers a set of N successive tracks of the same object. Consecutive observation windows are shifted by just 1 track, in order to mimic a real cataloging system and be able to apply the detection and estimation scheme to single tracks.

The N tracks in the observation window are compared to a reference orbit in terms of WRMS (see Subsection 2.1) to detect any possible maneuver. This orbit is computed with tracks belonging to the window of four simulation steps before, to avoid contamination of any undetected post-maneuver track. Hence, if an observation window contains tracks from number m to $m + N - 1$, the reference orbit is the one computed with tracks $m - 4$ up to $m + N - 5$. If no maneuver is detected, the orbit is updated via OD with the tracks inside the observation window. The OD relies on a high-fidelity numerical propagator discussed in Subsection 3.1. However, if a maneuver is detected, the track-to-orbit maneuver estimation algorithm is triggered with the reference orbit (i.e., pre-maneuver orbit), and an a-priori maneuver estimate is obtained. Maneuvers estimated are considered confirmed if involving four post-maneuver tracks, since only then the estimate is deemed to be sufficiently accurate for a first guess [5]. Then, the post-maneuver orbit is estimated via OD, adding the maneuver parameters (magnitude, direction and epoch) as estimated parameters with a-priori values coming from the initial guess. This is also done for maneuvers estimated with less than four

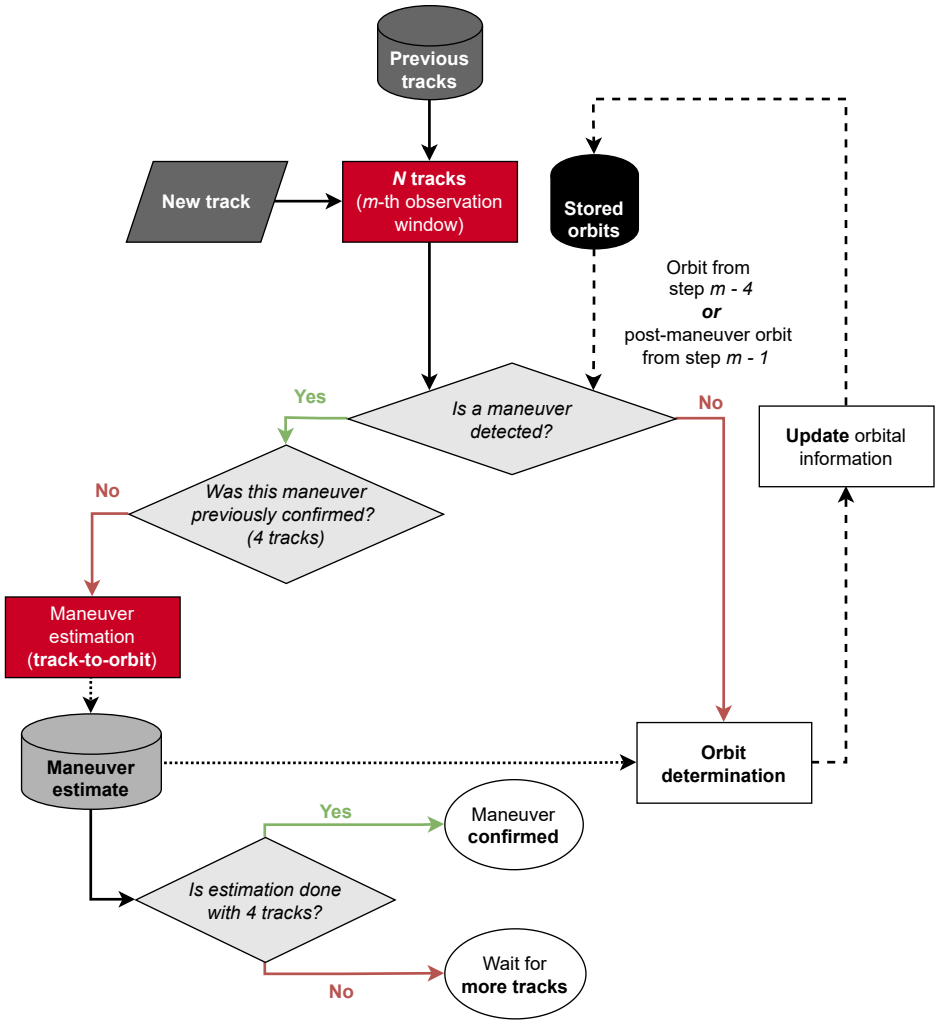

Figure 3: Catalog maintenance scheme accounting for maneuvers

tracks, but just to assess the impact of the number of tracks on the quality of the maneuver estimation, and the catalog is not updated in those cases.

Following the estimation of a post-maneuver orbit with four post-maneuver tracks, the orbit is propagated and compared to the tracks of the next observation window in the subsequent simulation step. If the residuals of the tracks do not trigger any maneuver detection, both the maneuver estimate and the post-maneuver orbit are taken as the new references and the processing is continued. However, if the residuals of the tracks leads to an additional maneuver detection, then the maneuver and post-maneuver orbit estimation are assumed not be reliable. In the simulation cases (presented in Section 3), this happens when trying to estimate long burn maneuvers (more than 10% of the orbital period).

The selection of 4 as the number of post-maneuver tracks for a maneuver to be confirmed as a reliable first guess is suggested from the analysis of the test cases. This choice is in-line with the results of literature regarding track-to-track associations [21], which states that 3 or 4 tracks are usually sufficient to obtain correct correlations. Similarly, in general at least 4 tracks are required for a full RSO initialization [24].

The refinement of the a-priori maneuver via OD is done by introducing a maneuver error on each direction, as well as a maneuver epoch error. These four parameters can be introduced in the orbit determination process by computing their transition-sensitivity product (namely, the partial derivatives of the measurements with respect to these errors, similarly to Equation (5)) and including their contributions for each observation in the normal equations matrix.

Note that the proposed approach is valid only for tracking activities. In survey activities, this process allows to establish a link between a set of uncorrelated tracks and an object represented by its cataloged orbit. The set of these links, or hypotheses, builds up an association tree, which grows as the number of track associations increases and they undergo the process of detection and estimation. The hypotheses needs to be merged, pruned and evaluated in order to finally promote the best correlation connecting the involved cataloged orbits and the processed observation data. The processing cost of this track-to-object correlation problem is determined by the combinations of track associations and objects, as for track-to-track association [21], hence the need of limiting this burden via computationally performing detection and estimation algorithms. This problem is not tackled in this paper.

3. Results

The following section presents results obtained by the application of the maneuver detection and estimation methodology. At first, Subsection 3.1 shows a test case to understand the level of accuracy of the dynamical models for the maneuver estimation algorithm. Subsection 3.2 briefly introduces the subject of the tests for the simulated cataloging chain, as well as some parameters used in the scenario. Subsection 3.3 describes the results of the application of the maneuver detection step, reporting its performances and underlining its limitations. Finally, Subsection 3.4 introduces the results of the maneuver estimation algorithm, assessing the impact of the number of post-maneuver tracks on quality, as well as the advantages obtained by performing the refinement with the high-fidelity orbit determination process.

3.1. Accuracy of the dynamical models

The dynamical models presented in Subsection 2.3 are tested to define their performances. They are compared against a high-fidelity numerical propagator, to determine the level of accuracy reached in the propagation, and among them, to assess the benefit of introducing the higher-order Keplerian dynamics with respect to the linear propagation via STM. The subject of the tests is a LEO object, whose characteristics are reported in Table 1. The position and velocity vectors are reported in the Geocentric Celestial Reference Frame (GCRF). The orbit of the satellite is propagated for a total of 5 days, considering a maneuver to happen after 1 day of simulation.

Table 1: Characteristics of satellite for the propagation accuracy test

Epoch	September 5^{th}, 2018, 00:00 UTC
Position r	$[3528.52,\ -4599.69,\ 4232.54]^T\ km$
Velocity v	$[-3.72,\ 2.59,\ 5.91]^T\ km/s$
Area-to-mass ratio	$10^{-2}\, m^2/kg$
Drag coeff.	3.334
SRP coeff.	0.967

To begin with, a first high-fidelity propagation is performed to generate the trajectory of $\mathbf{x}_A(t)$, required for the linear model and the Keplerian +

linear perturbations ones (with and without TNW corrections). The numerical propagator includes the force contributions reported in Table 2. A second propagation is carried out considering an impulsive maneuver equal to $[10,\ 10,\ 10]^T\ cm/s$ in the Radial – In-track – Cross-track (RIC) frame, generating $\mathbf{x}_B^{num}(t)$ (which is taken as a reference for comparison).

Table 2: Force models of the high-fidelity propagator

Gravity field	30×30
Third body perturbations	Moon, Sun and other planets
Tides	Solid tides only
Atmospheric drag	MSISE90 model
SRP	Cannonball model

The three simplified dynamical models are then used to compute trajectories considering the same maneuver. For sake of simplicity, the linear model (Equation (10)) will be referred to as *DM0*, the Keplerian + linear perturbations model (Equation (11)) will be named *DM1*, and finally the acronym *DM2* will be used for the propagator with TNW corrections (Equation (11)). The results of the test are presented in Figure 4 through the Root Mean Square Error (RMSE), in position and velocity components, of the difference between the high-fidelity and the approximated trajectories, namely the RMSE of $\mathbf{x}_B^{num}(t) - \mathbf{x}_{B,lin}(t)$, of $\mathbf{x}_B^{num}(t) - \mathbf{x}'_B(t)$ and of $\mathbf{x}_B^{num} - \mathbf{x}_B(t)$ (recalling their expressions in Equations (10), (11) and (13)). The difference in the position components is defined as $\Delta\mathbf{r}$, while the one for the velocity components is $\Delta\mathbf{v}$. The errors are averaged in rolling mean over sliding windows approximately equal to an orbital revolution of the satellite (computed at t_M after the maneuver) to filter out oscillations with the same period. In Figure 5, the RMSE of the dynamical models is normalized with respect to the true effect of the maneuver on the state, namely $\mathbf{x}_B^{num}(t) - \mathbf{x}_A(t)$. In each of the plots, the vertical dashed line represents the maneuver epoch.

Important differences can be noticed between the three dynamical models. DM0 starts diverging quite soon after the maneuver epoch, presenting an almost quadratic trend and reaching a final error of approximately 700 m in position and 0.7 m/s in velocity (both around 10^{-2} when normalized with respect to the effect of the maneuver) after four days. DM1 presents

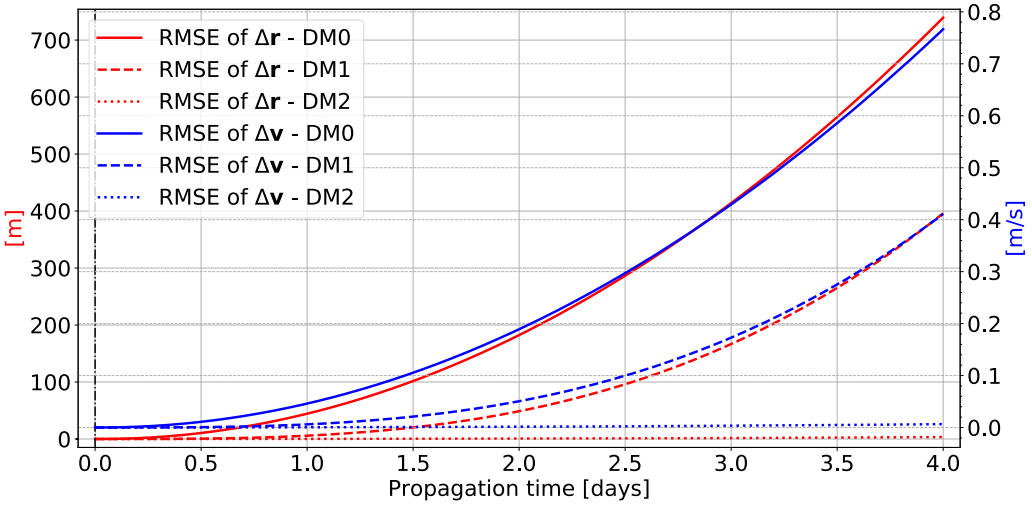

Figure 4: Test for propagation accuracy of the three dynamical models (RMSE)

a similar growth of the error, but the divergence is delayed with respect to the linear model (of approximately 1 day) and the final errors are lower than the previous case ($\approx 400\ m$ and $\approx 0.4\ m/s$). The best performances are, by far, the ones of DM2: in fact, no divergence of the propagation in the four days is spotted and the normalized errors do not exceed 10^{-4} in both position and velocity (being around $2\ m$ and $0.004\ mm/s$ in absolute terms). For our simulation scenario (whose details are reported in Subsection 3.2), 4 days are generally sufficient to receive 4 tracks from the object and so to perform a satisfactory estimation of a maneuver.

It is clear that a great advantage can be obtained by using DM2 instead of DM0, which was employed in [5]. In fact, the substantial improvement in accuracy can improve the quality of the maneuver estimates while not increasing considerably the computational cost of the estimation algorithm.

3.2. Simulation scenario setup

The subject of the tests in the simulation scenario is *Sentinel 3-A*, that is on a low-eccentricity polar orbit with a nominal altitude of 814 km and inclination of 98.65°. The time window considered for the simulation starts in 2017 and ends in 2019. The satellite performs a total of 22 maneuvers, with burn magnitude varying from a few mm/s to m/s. Maneuvers are either impulsive, with duration in the order of a few seconds, or long, with duration between 12 and 15 minutes (greater than 10% of the nominal orbital period

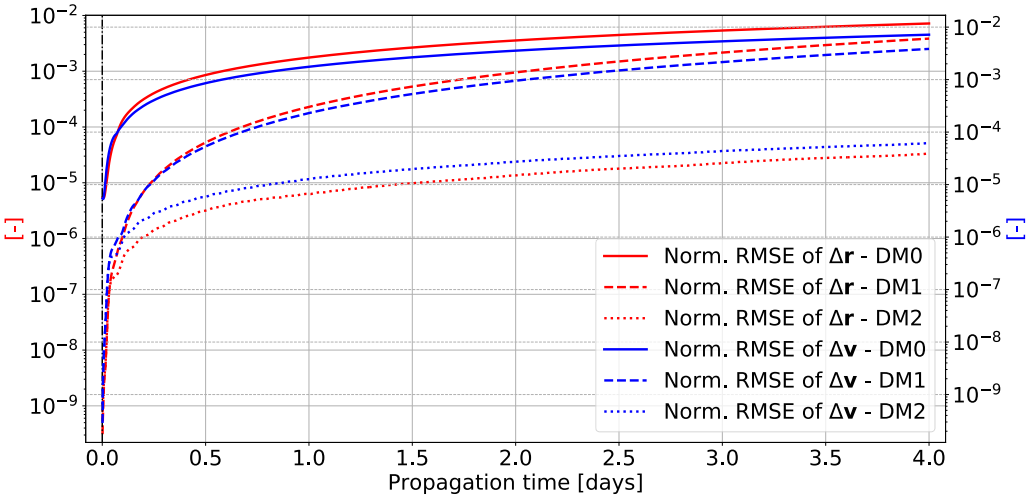

Figure 5: Test for propagation accuracy of the three dynamical models (normalized RMSE)

of the satellite, that is approximately 108 minutes). Both the initial orbit and maneuver history are publicly available [25] [26]. With such maneuver history, an orbit is propagated for the three years and simulated tracks are generated considering one radar located in mainland Spain, having a pyramidal field of view of 43.2° × 30° in semi-aperture. Zero-mean Gaussian noise is added to each observation in the tracks as with 1-sigma error of 5 m for range, 500 mm/s for range-rate and 300 $mdeg$ for angular measurements. The sensor is considered to be always operating and pointing towards the same direction. The observation windows at each simulation step include 18 tracks with a typical revisit frequency of 12 hours (as the satellite is on a polar orbit), yielding a time span equal or greater than 9 days. The reference pre-maneuver orbits are in general referred to 2 days before the last track in the window, as they are estimated with tracks of four simulation steps before (point 1 of the workflow in Subsection 2.4).

3.3. Maneuver detection

The primary and secondary thresholds to trigger maneuver detection are set to 5.0 and 2.5 respectively, compared to the typical expected value of the WRMS of 1.0 in a nominal OD. For the application of the secondary threshold, it has been selected a maximum of 14 hours to look for previous post-maneuver tracks. This value is slightly greater than the generic revisit

time of a the satellite. Consistently with detection theory, the following definitions are adopted:

- *True positives*: maneuvers that are correctly detected.
- *False positives*: maneuvers that do not occur but are still detected.
- *False negatives*: maneuvers that are not detected.

The selection of these thresholds for the WRMS metric proves to be robust for our tests. The algorithm reports a total of 29 maneuvers in the simulation time span: 22 of them are true positives (76% of the total), entailing a 0% of false negatives. The remaining 7 (24% of the total) are false positives, which are found to be triggered in cases with long burn times: the estimation of the post-maneuver orbit and of the maneuver itself can be poor and hence generate high track residuals in the subsequent simulation steps.

There are three cases where the first post-maneuver track is not immediately detected. This can be attributed to the fact that this is arriving close to the burn epoch and the corresponding maneuver has relatively low magnitude. Nevertheless, the information about these observations are recovered and employed for maneuver estimation as soon as the second post-maneuver track, detected via the primary threshold, arrives, thanks to the application of the lower secondary threshold.

The selected values for the thresholds and the number of past hours have proven to be effective in this simulated scenario, but that a tuning will be required in order to adapt the algorithm to a wider variety of cases. The extension of the methodology in the multi-target multi-sensor association framework will demand an augmentation of the detection scheme, capable of generating likely track-to-orbit correlations that will then be evaluated by the estimation algorithm.

3.4. Results for maneuver estimation

This subsection presents a set of results obtained by the application of the maneuver estimation algorithm, tested in the scenario using the dynamical model DM2, and of the subsequent refinement via high-fidelity OD. The selected discretization step for $t_M \in T$ is of 9 minutes, approximately 9% of the orbital period of the satellite. Subsection 3.4.1 presents some overall results obtained by the application of the two-step estimation, validating the process and showing how the estimation can improve with an increasing number of

post-maneuver tracks. This last aspect is also analyzed in Subsection 3.4.2, which presents a test case of the estimation of an impulsive maneuver, supporting the choice of taking 4 tracks to confirm a maneuver execution and that the selection strategy for the selection of the most suitable a-priori estimate is effective. Subsection 3.4.3 highlights the major limitation of the methodology, which is the estimation of long burns.

3.4.1. Overall results

This subsection presents an overview of the results obtained for the estimation of the 22 maneuvers performed in years 2017, 2018 and 2019 by Sentinel 3-A to discuss the overall performance of the proposed estimation methodology. Here, the two parameters considered to define the quality of the maneuvers estimates are the errors in the estimated vector and the estimated epoch. The distributions of such errors are shown in the figures in Tables 3 and 4. The smaller plots in each figure present the distribution (and the cumulative distribution function, CDF) of the solutions according to the relative magnitude error (on top) and the epoch error (on the right). The plots are presented for associations of an increasing number of post-maneuver tracks, from 1 to 4. If post-maneuver tracks are numbered in ascending temporal order as $\{1, 2, 3, 4\}$, the considered post-maneuver associations are $\{1\}$, $\{1, 2\}$, $\{1, 2, 3\}$ and $\{1, 2, 3, 4\}$. The graphs on the left side report the estimates coming from the estimation algorithm (using DM2), while those on the right side are the subsequent refinements of the a-priori guesses employing high-fidelity OD (Hi-Fi OD).

The distributions on the left side show that, for an increasing number of post-maneuver tracks, the error of the estimation algorithm (for both magnitude and epoch) tends to decrease, as well as the dispersion of the points. Associations of 1 track cannot be considered reliable since errors can reach very high values. The estimation is mediocre due to the low number of measurements involved and, at times, also because the track is received shortly after the maneuver, thus its modest divergence with respect to the pre-maneuver orbit is not captured by the algorithm (due to the noise of the measurements and the accuracy of the dynamical model). For associations of 2 tracks, errors can reach up to 300% in magnitude and 800 minutes in epoch, which drop to 150% and 150 minutes for 3 tracks, and finally to a maximum 75% and 100 minutes for 4 tracks. This confirms the choice of 4 as the number of post-maneuver tracks to confirm a reliable first maneuver guess (being in line with literature), since the errors are at their minimum and the dis-

persion of the points is the lowest among all associations. Nonetheless, also associations of 3 tracks can be eventually considered with larger uncertainty on the estimation. The outliers in terms of maneuver epoch correspond to long burns, which are not properly solved by the estimation algorithm, leading to ambiguities in the selection of the first estimate (see Subsection 3.4.3). It is worth to notice that the errors in the maneuver epoch are multiples or fractions of the orbital period of the satellite (approximately equal to 100 minutes). Associating more than 4 tracks could be beneficial; yet, it could possibly lead to poor estimations, since the dynamical model could start diverging for tracks far from the maneuver epoch in cases of higher magnitude burns. Moreover, the computational cost of the maneuver estimation algorithm would increase as more measurements are processed.

On the other hand, the distributions on the right side, related to high-fidelity orbit determination, show how the estimation errors and the dispersion can improve in the second iteration of the estimation process (excluding outliers). For all numbers of associated tracks, this step reduces both the error on magnitude and epoch, with a greater impact on the first one than on the second.

Table 3: Distribution of the estimation errors (associations of 1 and 2 tracks)

DM2	**Hi-Fi OD**
1 track	
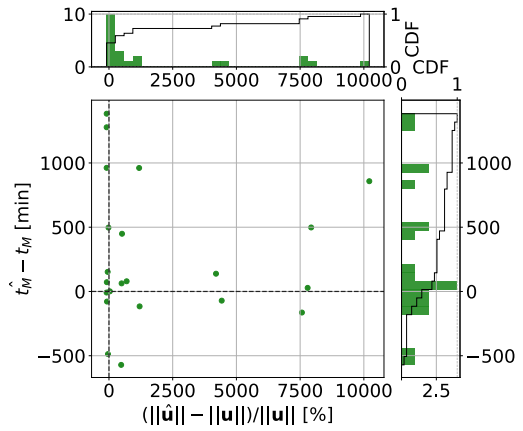	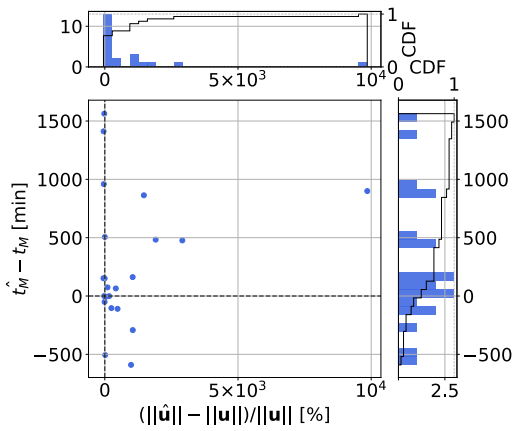
2 tracks	
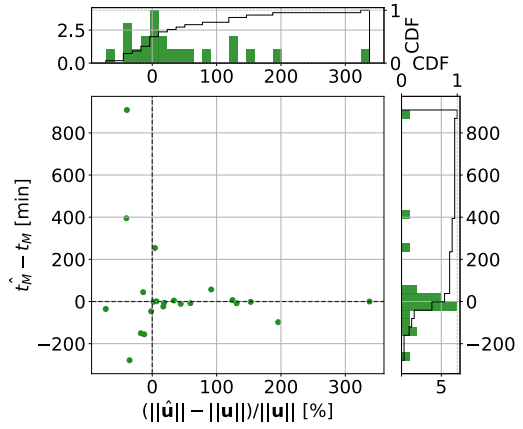	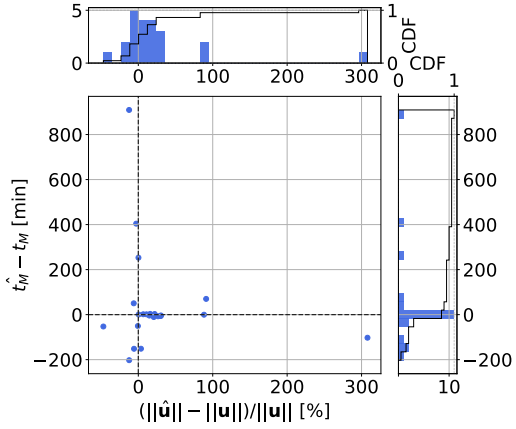

Table 4: Distribution of the estimation errors (associations of 3 and 4 tracks)

DM2	**Hi-Fi OD**
3 tracks	
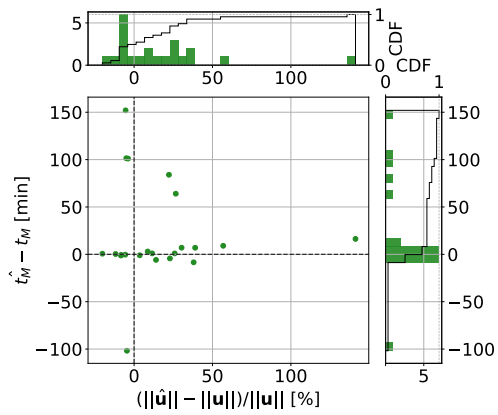	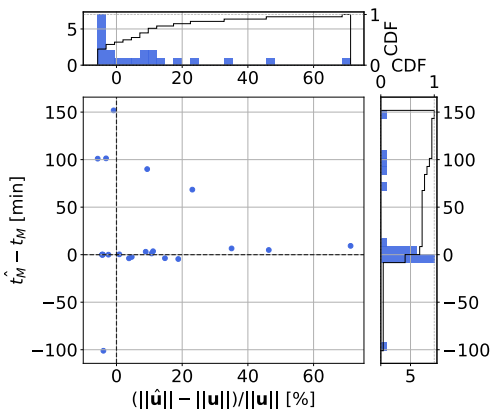
4 tracks	
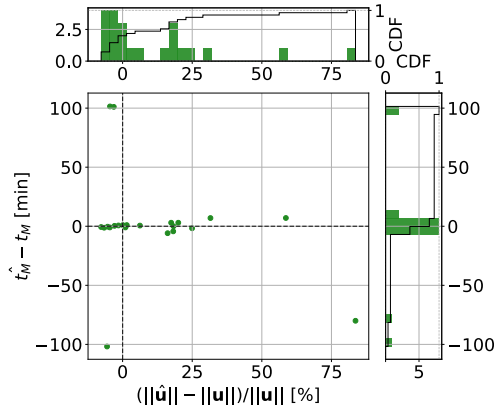	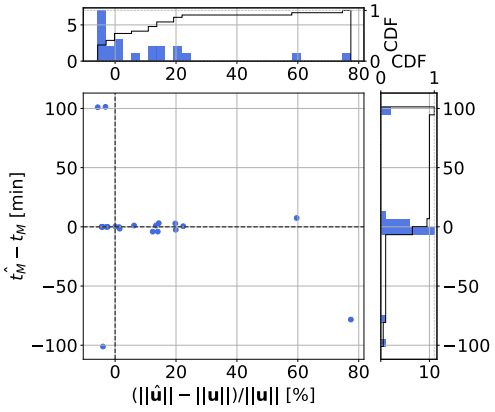

3.4.2. Short maneuver case

This subsection presents one test case taken from the 22 maneuvers (representing an impulsive burn). The characteristics of the true maneuver are reported in Table 5. The maneuver vector is reported in the RIC frame. The arrival times represent the time at which the simulated tracks, whose duration is approximately 2 minutes, become available. For sake of simplicity, the involved post-maneuver tracks are numbered sequentially in the set $\{1, 2, 3, 4\}$.

Table 5: Characteristics of maneuver on July 12$^{\text{th}}$, 2017

Maneuver epoch t_M	July 12$^{\text{th}}$, 2017, 09:44 UTC
Magnitude (RIC frame)	$[0.111, 5.590, 0.819]^T$ mm/s
Total Delta-V	5.65 mm/s
Duration	3 s
Arrival time of tracks	$t_M + 1\ h$, $t_M + 12\ h$, $t_M + 24\ h$, $t_M + 36\ h$

Figures 6 to 9 show the evolution of $\sqrt{J}$ and $\|\hat{\mathbf{u}}\|$ as a function of $t_M \in T$ for increasing number of associated tracks. The vertical dashed lines represent the true maneuver epoch and the estimated epoch $\hat{t}_M$. It is noticeable from Figure 6 that the maneuver estimation with a single track does not show any meaningful point nor pattern, both in terms of $\sqrt{J}$ and $\|\hat{\mathbf{u}}\|$. As mentioned before, the estimation turns out to be not satisfactory since few measurements are used and the track is received very shortly after the maneuver. Any solution computed with a single track is generally not considered to be reliable.

Figure 7 presents the results of the maneuver estimation algorithm with the association of the first two post-maneuver tracks $\{1, 2\}$. The plots are less noisy than the previous case and different minima can be spotted. The selected estimate has a very low epoch error (in the order of the time discretization step), but the estimated maneuver (approximately 10^{-2} m/s) is one order of magnitude greater than the true one.

The functions $\sqrt{J}$ and $\|\hat{\mathbf{u}}\|$ show a different trend when 3 tracks are considered (Figure 8). Both the WRMS and the maneuver magnitude now present clear regions of minima, which are in general not coinciding and are

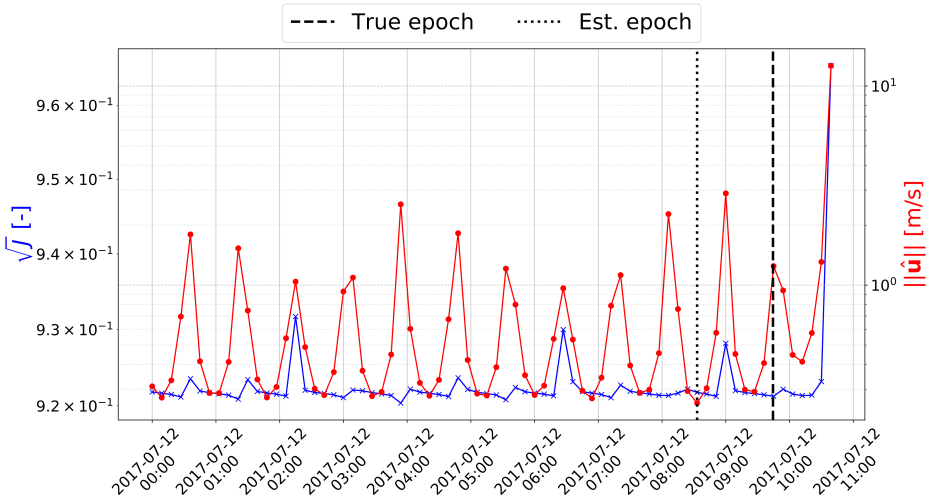

Figure 6: Initial estimation of maneuver on 12/07/2017 with tracks $\{1\}$

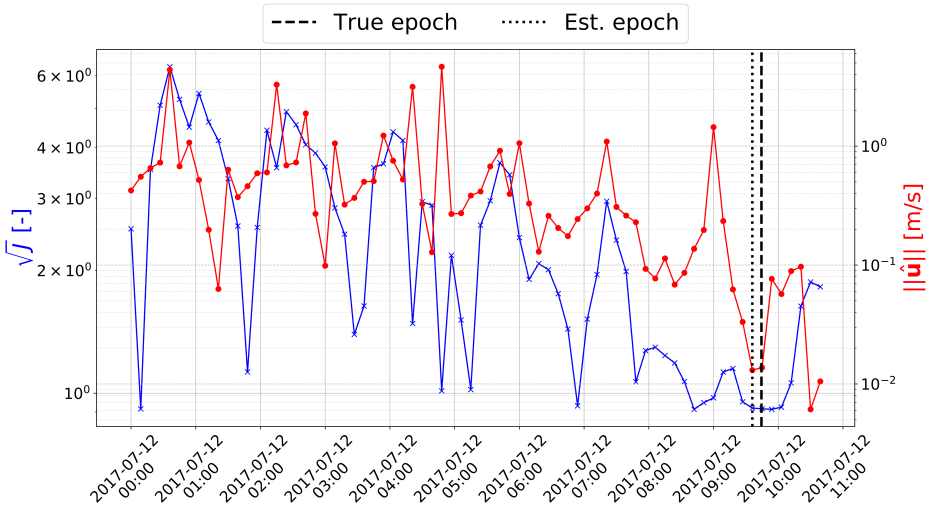

Figure 7: Initial estimation of maneuver on 12/07/2017 with tracks $\{1, 2\}$

separated by approximately 1.5 hours, i.e. one orbital period of the satellite. This repetitive pattern can be associated to the in-track nature of the maneuver. The non-linear behavior of the two functions and the dislocation of the minima suggests that a joint estimation of the maneuver vector and epoch estimation is not completely viable; additionally, it is the rationale

behind the decision of taking the optimal $\|\hat{\mathbf{u}}\|$ among the $\sqrt{J}$ minima in the selection strategy.

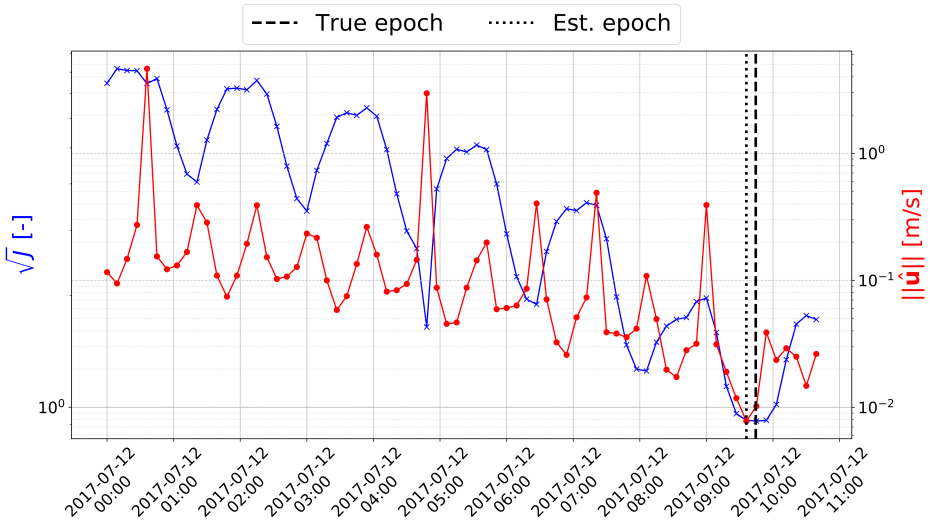

Figure 8: Initial estimation of maneuver on 12/07/2017 with tracks $\{1, 2, 3\}$

The estimation with an association of 4 tracks, presented in Figure 9, highlights a solution that is optimal both in terms of WRMS and maneuver magnitude. In this case, this minimum is exactly the chosen solution, being the most suitable estimate in the pool according to the proposed selection criterion. Its characteristics are reported in Table 6. The maneuver epoch is very well estimated (with an error of 1 minute, due to time discretization), as well as the in-track component of the maneuver, while errors are found on the radial and cross-track terms; nonetheless, the error in terms of magnitude (relatively to the true maneuver) is close to 6%. In this case, as the maneuver magnitude is modest, the accuracy of the method is limited by the noise introduced by the measurements. This estimate can be considered as a reliable first guess or initial estimate for the later complete estimation process.

Similar behaviors of $\sqrt{J}$ and $\|\hat{\mathbf{u}}\|$ as in Figure 9 are encountered in most of the test cases for associations with 4 post-maneuver tracks; differences appear as the true maneuver shifts toward a more radial or a more cross-track burn, which has an impact on the period of the minima. Exception is made for longer burns ($10 \div 15$ minutes), in which the two functions might not show

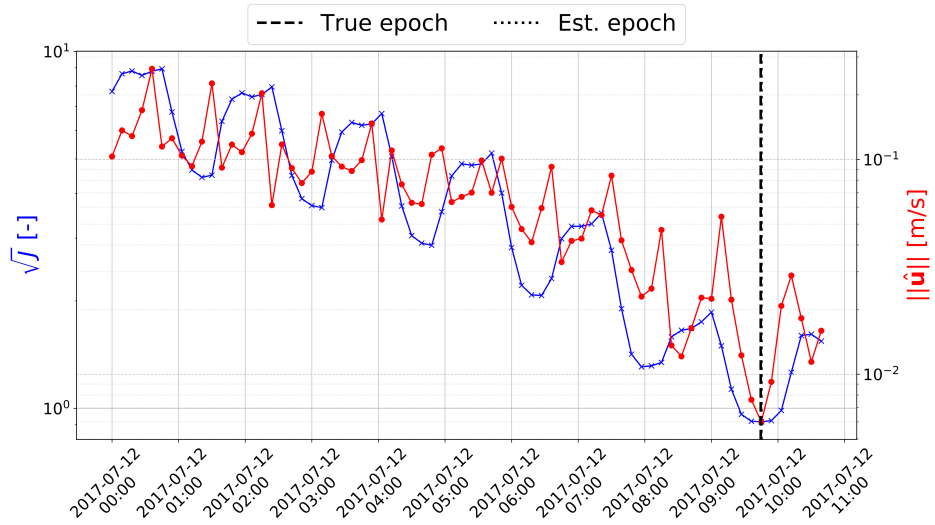

Figure 9: Initial estimation of maneuver on 12/07/2017 with tracks $\{1, 2, 3, 4\}$

Table 6: Characteristics of chosen estimate for maneuver on 12/07/2017 with tracks $\{1, 2, 3, 4\}$

Estimated $\hat{t}_M$	**Estimated $\hat{\mathbf{u}}$**	**Relative $\|\hat{\mathbf{u}}\|$ err.**
July 12^{th}, 2017, 09:45	$[0.997, 5.595, 1.931]^T$ mm/s	6.22 %

such clear patterns and the retrieved estimate can be unsatisfactory, both in terms of epoch and maneuver vector.

3.4.3. Long maneuver case

This subsection presents the result of the preliminary estimation of a long burn. The characteristics of the true maneuver are reported in Table 7. The maneuver vector is reported in the RIC frame. The involved post-maneuver tracks are numbered sequentially in the set $\{1, 2, 3, 4\}$. Figures 10 and 11 present the results of the application of the estimation for the association of tracks $\{1, 2, 3\}$ and $\{1, 2, 3, 4\}$.

It is possible to observe that the $\sqrt{J}$ and $\|\hat{\mathbf{u}}\|$ minima are separated by approximately 50 minutes, which is half the orbital period of the satellite, due to the greater cross-track component of the maneuver. In Figure 10, three minima with $\sqrt{J} < 4$ can be identified. Associating the 4^{th} does not

Table 7: Characteristics of maneuver on September 6^{th}, 2017

Maneuver epoch t_M	September 6^{th}, 2017 10:26 UTC
Real maneuver components	$[0.007,\ 0.014,\ 2.085]^T\ m/s$
Maneuver magnitude	$2.09\ m/s$
Maneuver duration	$13.5\ min$
Arrival time of tracks	$t_M + 24\ h$, $t_M + 36\ h$, $t_M + 48\ h$, $t_M + 60\ h$

help in evidencing these minima and in both cases there is no clear solution standing out, as opposed to the test case with an impulsive maneuver. It is also noticeable that the solution closest to the maneuver epoch is associated to a local $\sqrt{J}$ minimum but is not included in the selection pool since its value is greater than the 110% of the absolute minimum. The selection strategy for the most suitable estimate therefore fails for both associations. Table 8 reports the characteristics of the estimated maneuver. The error on the maneuver epoch is approximately 1.5 hours (or one orbital period), while the relative error with respect to the true maneuver is 5.58%. Even if the maneuver epoch is not correctly determined, the estimation of the magnitude is still valuable.

Table 8: Characteristics of chosen estimate for maneuver on 06/09/2017 with tracks $\{1, 2, 3, 4\}$

Estimated $\hat{t}_M$	**Estimated $\hat{\mathbf{u}}$**	**Relative $\|\hat{\mathbf{u}}\|$ err.**
Sept. 6^{th}, 2017, 08:51	$[-0.031,\ 0.013,\ 1.968]^T\ m/s$	5.58 %

As already mentioned, this result is due to the limited applicability of the maneuver estimation algorithm, which relies on an impulsive assumption. Nevertheless, since these long maneuvers are still detected, one possible way to overcome this problem would be estimating the maneuver duration as part of the high-fidelity orbit determination process once the a-priori values of maneuver time and magnitude have been computed based on the impulsive assumption.

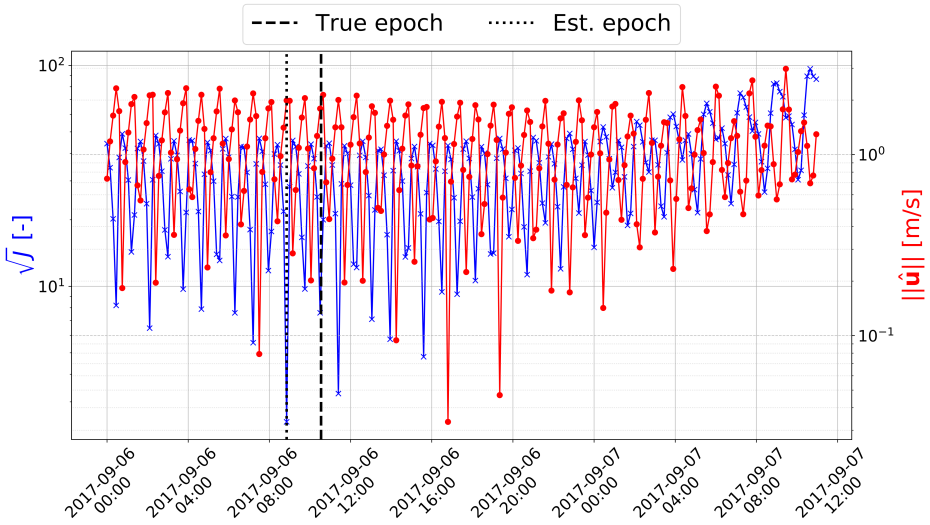

Figure 10: Initial estimation of maneuver on 06/09/2017 with tracks $\{1, 2, 3\}$

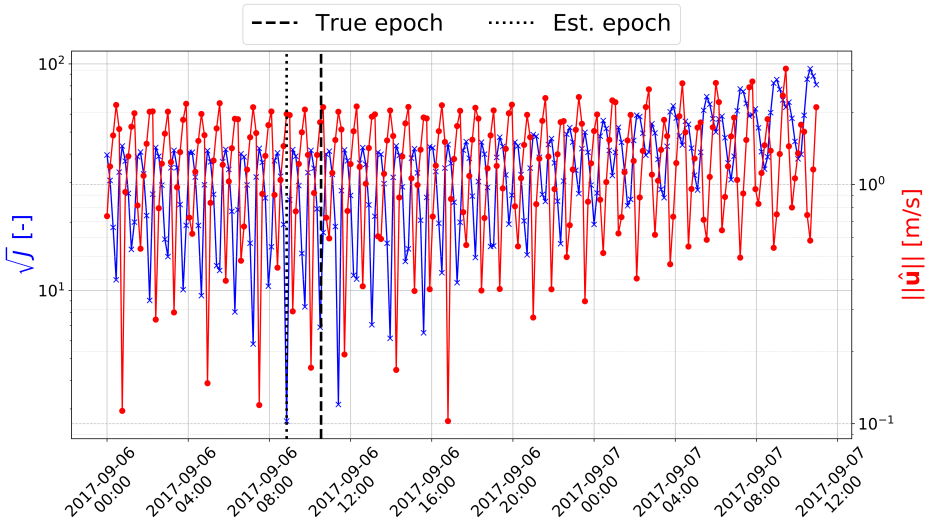

Figure 11: Initial estimation of maneuver on 06/09/2017 with tracks $\{1, 2, 3, 4\}$

4. Conclusions

A novel approach for maneuver detection and estimation, conceived for operational scenario, has been developed and tested for a single LEO satellite. The final goal of this methodology is to increase the performance of the cataloging chain and the robustness of the maintenance phase in the presence

of maneuvering targets. The detection strategy is based on metrics using the residuals of observations, while the estimation, cast as a track-to-orbit association problem, is a two-step process which employs a low-fidelity model at first, to obtain a first guess, and posterior high-fidelity orbit determination to refine the a-priori estimate and determine the post-maneuver orbit. The estimation algorithm was tested with the Keplerian + linear perturbations dynamical model (with TNW corrections), whose development was aimed at increasing the accuracy while keeping the computational cost low. This model is one of the major contributions of this work to the evolution of the previous publication [5], together with the strategy proposed to select the a-priori estimate among the pool of initial solutions. The detection and estimation algorithms are validated by tests run in a simulation scenario mimicking a cataloging maintenance chain for a single satellite. The approach proved to be robust at detecting maneuvers of the satellite and at providing reliable estimates, creating a link between an established pre-maneuver orbit and post-maneuver tracks. Results were presented and discussed for both the detection and estimation methodology. The first one was able to detect all the true maneuvers, while false maneuver triggering was only encountered after the estimation of long burns, evidencing the limitation of the maneuver estimation algorithm in these situations. It was shown that the maneuver estimation algorithm, along with the selection criterion based on WRMS and on the control effort (adapted from the previous GEO analysis), can provide satisfactory results as the number of associated post-maneuver tracks increases. In this regard, it was proven that considering 3 or 4 tracks is a sound compromise between estimation quality and computational time; however, to have a safer margin, a maneuver estimate is deemed to be reliable only if estimated with 4 tracks in the simulation chain. Moreover, the impact of the second estimation step, based on the a-priori estimate, is able to increase the accuracy for both maneuver vector and epoch, validating the proposed approach, as well as for the post-maneuver state prediction.

The detection strategy can be augmented by different metrics such as the median values of the WRMS, and by defining more secondary thresholds to increase robustness. Regarding the estimation algorithm, improvements can be achieved by increasing the accuracy of the propagation while keeping a relatively low computational effort. This can be done by including $J2$ as a perturbation term, a simple model for aerodynamic drag or even employing semi-analytical propagators. Moreover, a methodology that could be applied is the one of Multi Fidelity propagation, which is a concept already pre-

sented in maneuver detection and estimation literature [12]. The problem of estimating long burns would require a reassessment of the methodology, but a viable option would be to include the maneuver duration as a parameter in the high-fidelity OD, still employing the a-priori estimate based on the impulsive assumption as first guess.

Future works will tackle the extension and validation of the track-to-orbit maneuver detection and estimation methodology to a wider multi-target multi-sensor association framework, in which the goal will be to associate multiple maneuverable targets with their post-maneuver tracks. In addition, heuristics can be introduced in the problem by considering the statistical characterization of data regarding past maneuvers and typical maneuver patterns, as proposed in [17], [18], [19] and [20].

Acknowledgment

The corresponding author would like to mention that this work has been developed as part of an internship in the Space Situational Awareness section of the Flight Dynamics Operations and Systems business unit at GMV. The internship was devoted to the preparation of a M.Sc. thesis in Space Engineering, defended in April 2022 at Politecnico di Milano [27]. This research did not receive any specific grant from funding agencies in the public, commercial, or not-for-profit sectors.

References

[1] S. D. Office, Esa's annual space environment report, Tech. Rep. GEN-DB-LOG-00288-OPS-SD, ESOC, Darmstadt, Germany (04 2022).

[2] E. S. O. C. (ESOC), Discosweb (2021).
URL https://discosweb.esoc.esa.int/

[3] T. Kelso, Celestrak (1998).
URL https://celestrak.com/

[4] G. Peterson, M. Sorgeb, J. McVeyc, S. Gegenheimerd, G. Henninge, Tracking requirements in leo for space traffic management in the presence of proposed small satellites, in: 69th International Astronautical Congress, Bremen, Germany, 2018.

[5] A. Pastor, G. Escribano, M. Sanjurjo-Rivo, D. Escobar, Satellite maneuver detection and estimation with optical survey observations, The Journal of the Astronautical Sciences (2022). doi:https://doi.org/10.1007/s40295-022-00311-5.

[6] R. Patera, Space event detection method, Journal of Spacecraft and Rockets 45 (2008) 554–559. doi:10.2514/1.30348.

[7] T. Kelecy, D. Hall, K. Hamada, D. Stocker, Satellite Maneuver Detection Using Two-line Elements Data, in: Advanced Maui Optical and Space Surveillance Technologies Conference, 2007, p. E19.

[8] R. Vazquez, J. C. Sanchez, J. M. Montilla, J. Galan-Vioque, F. Gavilan, F. S. Lanagran, J. R. Benayas, F. A. R. Lopez, J. Siminski, C. P. Hernandez, Manoeuvre detection for near-orbiting objects, in: 8th European Conference on Space Debris, 2021.

[9] T. Kelecy, M. Jah, Detection and orbit determination of a satellite executing low thrust maneuvers, Acta Astronautica 66 (5-6) (2010) 798–809.

[10] G. M. Goff, J. T. Black, J. A. Beck, Tracking maneuvering spacecraft with filter-through approaches using interacting multiple models, Acta Astronautica 114 (2015) 152–163. doi:https://doi.org/10.1016/j.actaastro.2015.05.009.

[11] H. C. Ko, D. J. Scheeres, Orbit determination and maneuver detection using event representation with thrust-fourier-coefficients, in: Proceedings of the Advanced Maui Optical and Space Surveillance Technologies Conference, 2015.

[12] E. M. Zucchelli, Z. R. McLaughlin, B. A. Jones, Tracking maneuvering targets with multi-fidelity interacting multiple model filters, in: Proceedings of the Advanced Maui Optical and Space Surveillance Technologies Conference (AMOS), 2020.

[13] M. Holzinger, D. Scheeres, K. Alfriend, Object correlation, maneuver detection, and characterization using control distance metrics, Journal of Guidance, Control, and Dynamics 35 (2012) 1312–1325. doi:10.2514/1.53245.

[14] N. Singh, J. Horwood, A. Poore, Space object maneuver detection via a joint optimal control and multiple hypothesis tracking approach, in: 22nd AAS/AIAA Space Flight Mechanics Meeting, 2012.

[15] R. Serra, C. Yanez, C. Frueh, Tracklet-to-orbit association for maneuvering space objects using optimal control theory, Acta Astronautica 181 (2021) 271–281. doi:https://doi.org/10.1016/j.actaastro.2021.01.026.

[16] A. Milani, G. F. Gronchi, M. De' Michieli Vitturi, Z. Knezevic, Orbit determination with very short arcs. i - admissible regions, Celestial Mechanics and Dynamical Astronomy 90 (2004) 57–85. doi:10.1007/s10569-004-6593-5.

[17] J. Siminski, H. Fiedler, T. Flohrer, Correlation of observations and orbit recovery considering maneuvers, in: AAS/AIAA Space Flight Mechanics, 2017.

[18] J. Siminski, T. Flohrer, T. Schildknecht, Assessment of post-maneuver observation correlation using short-arc tracklets, in: 7th European Conference on Space Debris, 2017.

[19] G. Escribano, M. Sanjurjo-Rivo, J. Siminski, A. Pastor, D. Escobar, Maneuver detection via combined heuristical and statistical methodologies, in: 8th European Conference on Space Debris, 2021.

[20] G. Escribano, M. Sanjurjo-Rivo, J. Siminski, A. Pastor, D. Escobar, Automatic maneuver detection and tracking of space objects in optical survey scenarios based on stochastic hybrid systems formulation, Advances in Space Research 69 (9) (2022) 3460–3477. doi:https://doi.org/10.1016/j.asr.2022.02.034.

[21] A. Pastor, M. Sanjurjo-Rivo, D. Escobar, Track-to-track association methodology for operational surveillance scenarios with radar observations, CEAS Space Journal (2022).

[22] K. Kaminski, M. Zołnowski, E. Wnuk, J. Golebiewska, M. Kruzynski, M. Kaminska, M. Gedek, Low leo optical tracking observations with small telescopes, in: Proceedings of the 1st NEO and Debris Detection Conference, Darmstadt, Germany, 2019, pp. 22–24.

[23] O. Montenbruck, E. Gill, Satellite Orbits: Models, Methods, and Applications, Physics and astronomy online library, Springer Berlin Heidelberg, 2000.

[24] K. Hill, C. Sabol, K. T. Alfriend, Comparison of covariance based track association approaches using simulated radar data, The Journal of the Astronautical Sciences 59 (1) (2012) 281–300.

[25] E. Copernicus, Sentinel online - sentinel 3-a orbit description (2022).
URL https://sentinels.copernicus.eu/web/sentinel/missions/sentinel-3/satellite-description/orbit

[26] E. Copernicus, Sentinel online - sentinel 3-a satellite parameters for pod (2022).
URL https://sentinels.copernicus.eu/web/sentinel/technical-guides/sentinel-3-altimetry/pod/satellite-parameters

[27] L. Porcelli, Satellite manoeuvre detection and estimation with radar observations, Master's thesis, Politecnico di Milano - Dipartimento di Scienze e Tecnologie Aerospaziali (DAER) (2022).